

Systematic behavior of octupole states in deformed rare earth nuclei and the interacting boson approximation

P. D. Cottle

Department of Physics, Florida State University, Tallahassee, Florida 32306

N. V. Zamfir

Brookhaven National Laboratory, Upton, New York 11973;

Clark University, Worcester, Massachusetts 01610;

WNSL, Yale University, New Haven, Connecticut 06520;

and Institute of Atomic Physics, Bucharest-Magurele, Romania

(Received 26 March 1996)

A method for setting ϵ_f , one of the parameters in the interacting boson approximation-1 (IBA-1) with one f boson, by using the systematic behavior of the centroids of observed $E3$ strength is proposed and applied to obtaining fits for octupole bands in the deformed rare earth region. The ordering of bands with different K values, $B(E3)$ strengths and $B(E1)$ values are well reproduced. The calculations are in good agreement with the data in nearly all the $K=0, 1,$ and 2 octupole bands examined here. The least satisfactory fits were obtained for the $K^\pi=0^-$ bands in $^{160,162}\text{Dy}$. It is predicted that in $^{160,162,164}\text{Dy}$, ^{168}Er , and ^{172}Yb the $K=3$ octupole states based on the ground state and having significant $E3$ strength are above 6 MeV and are strongly fragmented. These results are quite different from predictions made previously. [S0556-2813(96)04007-1]

PACS number(s): 21.10.Re, 21.60.Fw, 23.20.Lv, 27.70.+q

I. INTRODUCTION

In spherical nuclei, a single collective $J^\pi=3^-$ low energy octupole state (LEOS) occurs at an energy below 4 MeV. In a nucleus with a stable quadrupole deformation, the LEOS is fragmented into four states having $K^\pi=0^-, 1^-, 2^-,$ and 3^- , where K is the projection of the octupole phonon's angular momentum on the symmetry axis of the nucleus. The distribution of the $E3$ strength (which is concentrated in the single 3^- state in a spherical nucleus) among the four 3^- states corresponding to the four K values varies from nucleus to nucleus and depends on the microscopic structure of the individual 3^- states as well as the Coriolis interaction between the states.

Barfield, Wood, Barrett, and Scholten [1] demonstrated that the interacting boson approximation-1 (IBA-1) (in which proton and neutron bosons are not distinguished) provides a straightforward framework for interpreting octupole vibrational behavior in the well-deformed rare earth nuclei. The authors of [1] were able to reproduce energies of octupole states and $E3$ strength distributions for nine nuclei in this region, but noted that considerable variations occurred in the values of several of the parameters. In the present work, we focus on one of these parameters, ϵ_f , which is the energy associated with the f boson. We interpret ϵ_f in a directly physical way as the energy of the LEOS. Since the LEOS is fragmented in deformed nuclei, we take the energy of the LEOS (and therefore ϵ_f) in a deformed nucleus to be the centroid of the octupole strength, which is given by [2]

$$C = \frac{\sum_i E_i B(E3; 0_{gs}^+ \rightarrow 3_i^-)}{\sum_i B(E3; 0_{gs}^+ \rightarrow 3_i^-)}. \quad (1)$$

The quality of the data on the distribution of octupole strength varies from nucleus to nucleus, so we set ϵ_f in in-

dividual nuclei by using the systematic behavior of the observed centroids of $E3$ strength in the deformed rare earth nuclei, instead of relying on the data in individual nuclei. (In contrast, Barfield *et al.* [1] set ϵ_f so as to make the average energy of the calculated bandheads the same as the experimental average, without any reference to the distribution of $E3$ strength.) With this prescription for ϵ_f , we fit the experimental data on energies, $E3$ strength distributions, and $E1$ transition strengths for the $K^\pi=0^-, 1^-,$ and 2^- bands of eight even-even deformed rare earth nuclei. Considerable data are available for these octupole bands, and we are able to satisfactorily reproduce nearly all of the available data. Finally, we use these calculations to predict the behavior of $K^\pi=3^-$ octupole bands, for which little experimental data are available. We predict that in several deformed rare earth nuclei the $E3$ strength associated with $K^\pi=3^-$ octupole states is located at energies above 6 MeV, the energy range usually associated with the low energy octupole resonance (LEOR) [3].

II. OCTUPOLE STATES IN THE IBA-1 AND THE PARAMETER ϵ_f

Octupole states are described in the IBA-1 by adding a single f boson with $L=3$ to the usual s - d boson model space [4,5]. The total number of s , d , and f bosons is conserved, and the number of f bosons, n_f , can be zero or one, for positive and negative parity states, respectively. The Hamiltonian is

$$H = H_{sd} + H_f + V_{sdf}, \quad (2)$$

where H_{sd} describes the positive parity core, H_f is the f -boson Hamiltonian, and V_{sdf} describes the f - sd interac-

tion. The sd core Hamiltonian used here is the ‘‘consistent- Q ’’ Hamiltonian, which was proposed in [6] and used in [1]:

$$H_{sd} = a_1 L_d \cdot L_d + a_2 Q_d \cdot Q_d, \quad (3)$$

where

$$L_d = \sqrt{10}(d^\dagger \tilde{d})^{(1)}, \quad (4)$$

$$Q_d = (s^\dagger \tilde{d} + d^\dagger s) + \chi_2 (d^\dagger \tilde{d})^{(2)}. \quad (5)$$

The f -boson Hamiltonian, H_f , is given by

$$H_f = \epsilon_f n_f, \quad (6)$$

where ϵ_f is the f -boson energy. The interaction term V_{sdf} used here is identical to that used in [1]:

$$V_{sdf} = A_1 L_d \cdot L_f + A_2 Q_d \cdot Q_f + A_3 :E_{df}^+ E_{df}:, \quad (7)$$

where

$$L_f = 2\sqrt{7}(f^\dagger \tilde{f})^{(1)}, \quad (8)$$

$$Q_f = -2\sqrt{7}(f^\dagger \tilde{f})^{(2)}, \quad (9)$$

$$:E_{df}^+ E_{df}: = 5:(d^\dagger \tilde{f})^{(3)} \cdot (f^\dagger \tilde{d})^{(3)}:. \quad (10)$$

In [1], the parameter ϵ_f was determined so as to make the average energy of the calculated bandheads the same as the corresponding experimental average. Here we propose another physical interpretation for ϵ_f , that it is equal to the octupole phonon energy, which is given by the energy centroid of $E3$ strength. To set ϵ_f in each nucleus we used the systematic behavior of the observed energy centroids so that inaccuracies introduced by the poor quality of data in single nuclei are minimized.

The systematic behavior of the octupole centroids for the $N=82-126$ major shell is shown in Fig. 1. This information comes from inelastic scattering and Coulomb excitation measurements performed with protons, deuterons, and alpha particles. Experimental studies in which more than one 3^- state was measured were included. There are experimental errors inherent in the measurements of the $B(E3; 0_{gs}^+ \rightarrow 3^-)$ values, and these translate into errors in the centroid energies. However, these errors are always less than 45 keV, so we have not included them in the figures. In $^{206,208}\text{Pb}$ [19,20], 3^- states at energies of 3.5 MeV and higher have been measured. These high energy states are probably associated with the LEOR. To exclude fragments of the LEOR as much as possible in these nuclei, we do not include 3^- states with energies higher than $(20 \text{ MeV})/A^{1/3}$, which is the lowest energy for this resonance included in the compilation of Kirson [3]. In other nuclei, we include all 3^- states, even if they are not assigned to octupole bands by the experimenters. There is some variation in the quality of the data; however, the compilation is sufficient for the purposes of the present work.

The centroid energies for $N=82-126$ are graphed against neutron number N in Fig. 1(a). A clear systematic trend is evident in the graph. From the beginning of the major shell ($N=82$), the centroid energy decreases, reaching a minimum near $N=90$. The energy then appears to increase

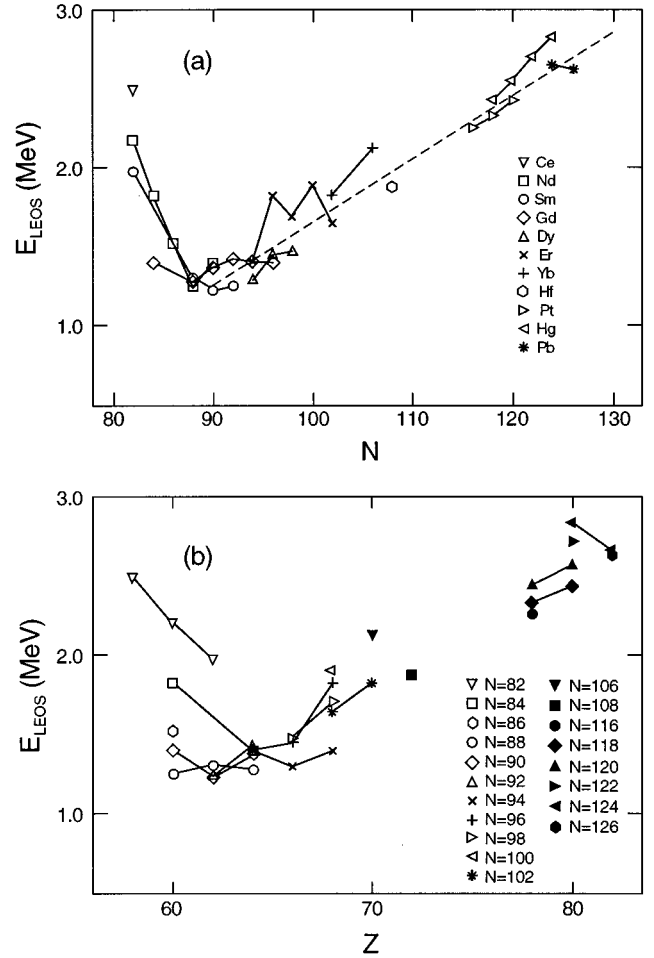


FIG. 1. Octupole centroids graphed against (a) the neutron number N and (b) the proton number Z . The data are from [2,7–20] and the dashed line shown in (a) is discussed in the text.

in a uniform way all the way to $N=126$, although there are no data for $N=110-114$. This behavior can be explained in terms of a schematic description of octupole states. In spherical nuclei, octupole states consist primarily of two quasiparticle excitations involving the unique parity orbit and the common parity orbit with three fewer units of both total and orbital angular momentum than the unique parity orbit. For the $N=82-126$ major shell, the relevant neutron orbits are $i_{13/2}$ and $f_{7/2}$. Near $N=82$, the $f_{7/2}$ orbit is actually the lowest in the major shell. As neutrons are added at the beginning of the shell, the $f_{7/2}$ orbit fills and the energy of the octupole state falls. When the $f_{7/2}$ orbit is filled near $N=88$, the Fermi surface is located between the $f_{7/2}$ and $i_{13/2}$ orbits and the energy of the octupole state reaches a minimum. At this point, the $i_{13/2}$ orbit begins to fill and the energy of the octupole state (or centroid of octupole states) begins to increase, and continues to increase until $N=126$. The onset of quadrupole deformation at $N=90$ results in the breaking of the degeneracies of the magnetic substates of the single-particle orbits; however, the centroids of the orbits remain roughly the same, and this general description of the behavior of the octupole centroid remains valid, even in deformed nuclei.

In Fig. 1(b), the octupole centroid energies are graphed

against Z . The trends in the graph, while at first not as clear as those in Fig. 1(a), are nevertheless useful for understanding the underlying microscopic structure of the octupole excitations. The unique parity orbit in the valence proton ($Z=50-82$) shell is $h_{11/2}$, and the common parity orbit with angular momentum three units less is $d_{5/2}$. Near the $N=82$ shell closure, there is a large gap at $Z=64$ [21]. The $d_{5/2}$ orbit lies below and $h_{11/2}$ above the gap. Near $N=90$, the energy of the $h_{11/2}$ proton orbit drops, closing the $Z=64$ gap.

For $N=82$ and 84 , the separation of the $d_{5/2}$ and $h_{11/2}$ proton orbits produces a sharp minimum in the energy of the octupole state at $Z=64$, where the $d_{5/2}$ orbit is full and the $h_{11/2}$ orbit is empty. Close to $N=90$, the gap between the $d_{5/2}$ and $h_{11/2}$ orbits closes, so that the minimum in the octupole centroid energy is not so pronounced. However, the general trend is still clear: the energy of the octupole state (or centroid) decreases as protons are added early in the shell, reaching a minimum near $Z=64$. As more protons are added past $Z=64$, the occupation of the $h_{11/2}$ orbit increases and the energy of the octupole state (centroid) increases as well. This trend can be seen all the way to the end of the proton shell near $Z=82$.

While there are clear systematic trends with respect to both N and Z , the variation with N is clearer, and we use this relationship between the octupole centroid energy and the neutron number to set ϵ_f . The dashed line drawn in Fig. 1(a) from $N=90$ to $N=126$ is given by the equation

$$E_{\text{LEOS}} = [(0.040) \times N - 2.35] \text{ MeV}. \quad (11)$$

This equation gives a reasonable description of the systematic behavior of octupole centroids above $N=90$ and provides a prescription for ϵ_f (with $\epsilon_f = E_{\text{LEOS}}$).

III. CALCULATIONS OF ENERGIES AND $B(E3)$ VALUES FOR $K^\pi=0^-, 1^-, 2^-$ BANDS

A considerable amount of data is available for $K^\pi=0^-, 1^-, 2^-$ octupole vibrational bands in some even-even deformed rare earth nuclei, so we attempted to reproduce much of the information available on these bands. Calculations using the IBA-1 with an f boson were performed for the $K^\pi=0^-, 1^-, 2^-$ bands of eight nuclei: ^{154}Sm , $^{156,158}\text{Gd}$, $^{160,162,164}\text{Dy}$, ^{168}Er , and ^{172}Yb . These nuclei were selected because energy and $B(E3)$ information was available for at least two of the these bands in each nucleus.

One important characteristic of this set of nuclei is that it includes isotopes with several different orders of octupole bands. In the beginning of the deformed region, the band sequence is $K^\pi=0^-, 1^-, 2^-$. As the Fermi level increases, the sequence changes to $1^-, 0^-, 2^-$ and then to $2^-, 1^-, 0^-$ [22]. Figure 2 illustrates the evolution of the band ordering with the fractional filling of the shell. Each isotope considered in the present study is schematically located. For example, ^{154}Sm is in the beginning of the deformed region and the ordering of the K bands is $0^-, 1^-, (2^-)$. As the number of active particles in increased, the order becomes $1^-, 0^-, 2^-$ as in ^{158}Gd and then $2^-, 1^-, 0^-$ as in ^{160}Dy . Past midshell, the increasing of Z and/or N leads to a decrease in the number of active holes and, consequently, to a decrease in the fractional filling

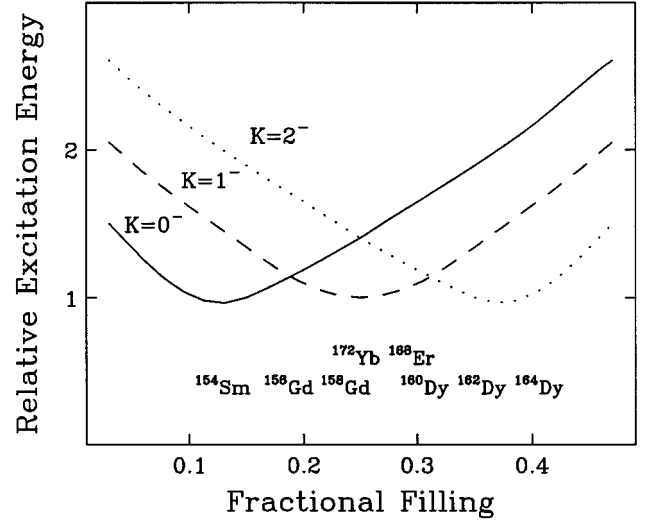


FIG. 2. Schematic illustration of the energies of the $K^\pi=0^-, 1^-, 2^-$ octupole vibrational bands as a function of the fractional filling of the proton and neutron valence shells. The approximate locations of the nuclei which are shown here generally reproduce the observed ordering.

in the shell, as in ^{168}Er , where the order is $1^-, 2^-, 0^-$, and ^{172}Yb , where Z is still larger (and the fractional filling is yet smaller) and the band order is $1^-, 0^-, 2^-$. Two of the isotopes studied here have two K bands which are almost degenerate: 0^- and 1^- in ^{156}Gd ; and 1^- and 2^- in ^{160}Dy . Strong mixing effects are present in both these cases. The characteristic evolution of the ordering of the octupole vibrational bands is also reflected in the level staggers in the different bands [23].

The Hamiltonian used here was discussed in Sec. II. The $E2$ operator used for both positive and negative parity states is that proposed in [6] and used in [1]:

$$T(E2) = e_2 Q_d. \quad (12)$$

The $E3$ transition rates are calculated with the operator [1]

$$T(E3) = e_3 [s^\dagger \tilde{f} + \chi_3 (d^\dagger \tilde{f})^{(3)} + \text{H.c.}], \quad (13)$$

where e_3 is the boson octupole effective charge. The computer codes used for these calculations were PHINT and FBEM [24]. Band assignments for states calculated in the model are made on the basis of calculated $B(E2)$ transitions.

Of the eight nuclei examined here, six were also included in the study of Barfield *et al.* [1]. The parameters used here for the positive parity states for these six nuclei are taken from Barfield *et al.*, who determined them in the following way: The parameters a_1 and a_2 were determined by fitting the ground state and gamma bands, and the quadrupole parameter χ_2 was determined from the experimental ratio $B(E2; 2_2^+ \rightarrow 0_{gs}^+) / B(E2; 2_1^+ \rightarrow 0_{gs}^+)$ as described in [6]. For the two nuclei studied here that were not studied in [1], the same procedure was followed to determine parameters for the positive parity states. The parameters for the positive parity states are given in Table I.

TABLE I. Parameters in H_{sd} .

| Nucleus | N_B | a_1 (keV) | a_2 (keV) | χ_2 |
|-------------------|-------|-------------|-------------|----------|
| ^{154}Sm | 11 | 0.0 | -36.0 | -0.72 |
| ^{156}Gd | 12 | 2.0 | -32.5 | -0.54 |
| ^{158}Gd | 13 | 3.0 | -27.5 | -0.63 |
| ^{160}Dy | 14 | 4.5 | -23.5 | -0.51 |
| ^{162}Dy | 15 | 6.0 | -20.0 | -0.54 |
| ^{164}Dy | 16 | 6.0 | -15.0 | -0.54 |
| ^{168}Er | 16 | 6.5 | -17.5 | -0.49 |
| ^{172}Yb | 16 | 4.5 | -22.5 | -0.80 |

There are four parameters which affect the calculations of the energies of the negative parity states (after the positive parity states have been set): ϵ_f [Eq. (6)], and A_1 , A_2 , and A_3 [Eq. (7)]. The parameter ϵ_f is set with the prescription described in Sec II. Once this is set, the structure is primarily given by the parameters A_2 and A_3 . The ratio A_2/A_3 determines the ordering of the octupole bands of different K values. Values for these parameters are listed in Table II. For reasonable values of A_1 , the $A_1 L_d \cdot L_f$ term in Eq. (7) has little influence on energy values. This term has no influence on wave functions and consequently does not affect the transition probabilities. Given these facts, we have left $A_1 = 0$ for the calculations here.

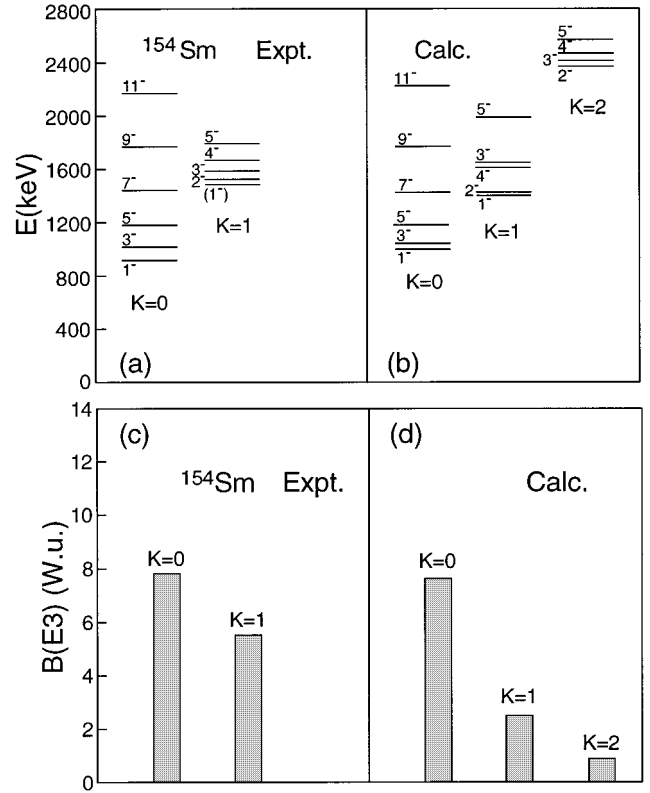
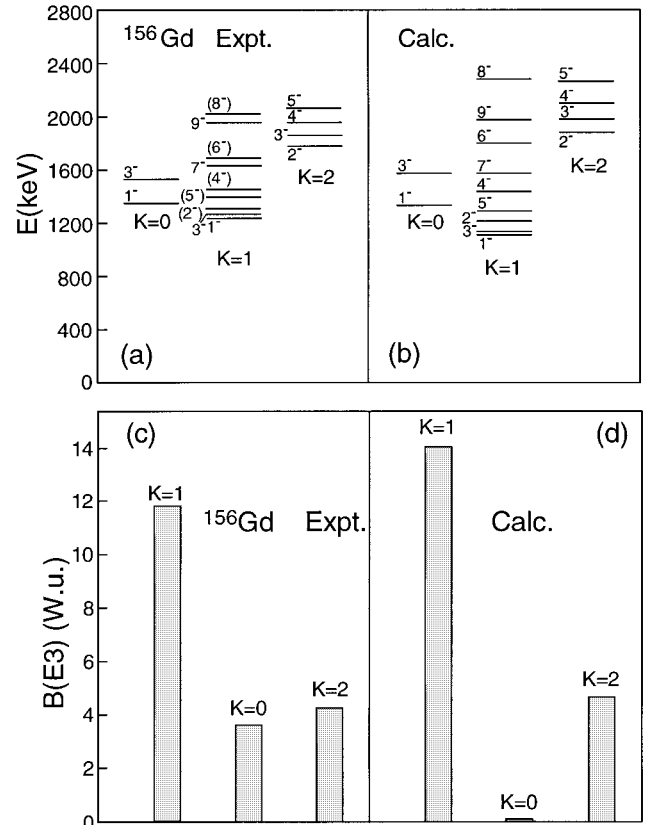
Calculations of the $B(E3; 0_{gs}^+ \rightarrow 3^-)$ transition probabilities depend on two parameters, e_3 and χ_3 . We found that a single value of e_3 ($0.20 eb^{3/2}$) was sufficient to describe the $E3$ transitions examined here. There was some variation in χ_3 ; however, it was considerably less than that found in [1]. The values of χ_3 are listed in Table II.

The results for the energies of octupole band states and the distribution of $E3$ strength among the octupole bands are given in Figs. 3–10. The experimental data shown in these figures are taken from [11,13–16,25–33]. For most of the nuclei shown here (^{154}Sm , $^{156,158}\text{Gd}$, ^{168}Er , and ^{172}Yb) the calculations reproduce the data well, although the fits are not quite as good at the higher spins in some of the bands. The difficulty in fitting higher spin states might be attributable to the alignment of the octupole phonons, as discussed by Vogel [34].

The fits to the energies in $^{160,162,164}\text{Dy}$ are not as good, particularly for the $K^\pi = 0^-$ bands. The deviation is greatest in ^{162}Dy , in which the calculated energy for the $J^\pi = 1^-$ bandhead of the $K^\pi = 0^-$ band is 900 keV higher than the experimental value. Barfield *et al.* [1] encountered the same

TABLE II. Parameters in H_f , V_{sdf} , $T(E3)$, and $T(E1)$.

| Nucleus | ϵ_f (keV) | A_2 (keV) | A_3 (keV) | χ_3 | χ_1 | χ'_1 |
|-------------------|--------------------|-------------|-------------|----------|----------|-----------|
| ^{154}Sm | 1.33 | -50 | 0 | 0.00 | -0.030 | -0.058 |
| ^{156}Gd | 1.33 | -70 | -134 | -0.38 | -0.026 | -0.054 |
| ^{158}Gd | 1.41 | -75 | -150 | +0.38 | -0.025 | -0.050 |
| ^{160}Dy | 1.41 | -60 | -260 | +1.13 | -0.025 | -0.050 |
| ^{162}Dy | 1.49 | -40 | -290 | +1.13 | -0.024 | -0.048 |
| ^{164}Dy | 1.57 | -22 | -312 | +1.13 | -0.022 | -0.044 |
| ^{168}Er | 1.65 | -60 | -190 | +0.76 | -0.023 | -0.044 |
| ^{172}Yb | 1.73 | -83 | -220 | +1.13 | -0.023 | -0.046 |

FIG. 3. Experimentally observed [11,26] and calculated octupole band energies and $B(E3; 0_{gs}^+ \rightarrow 3^-)$ values in ^{154}Sm .FIG. 4. Similar to Fig. 3 for ^{156}Gd [13,25,27].

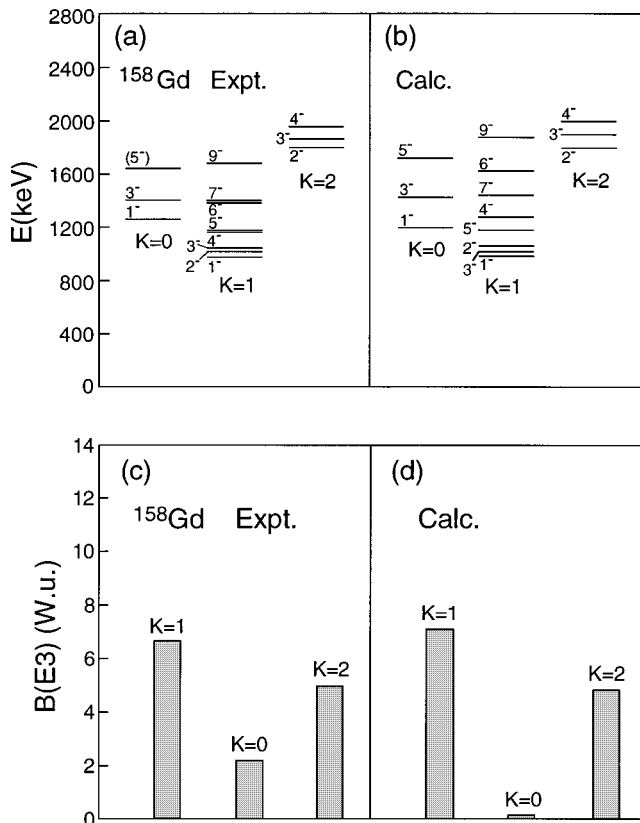


FIG. 5. Similar to Fig. 3 for ^{158}Gd [13,28].

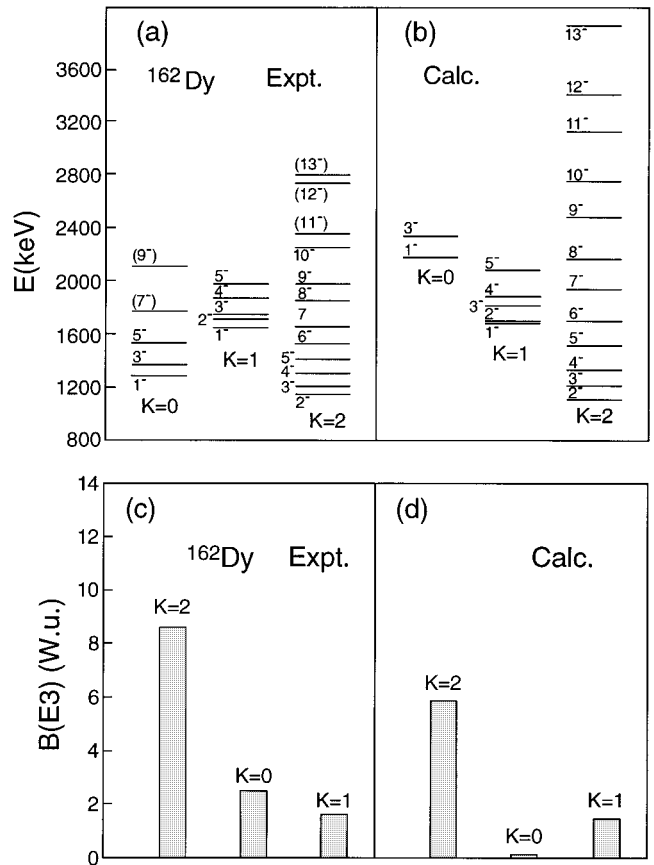


FIG. 7. Similar to Fig. 3 for ^{162}Dy [14,30].

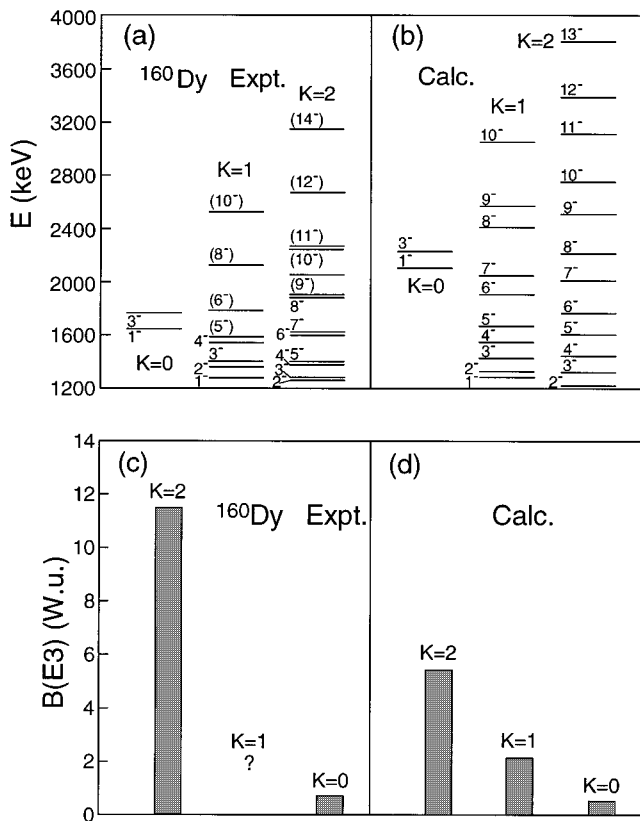


FIG. 6. Similar to Fig. 3 for ^{160}Dy [14,29].

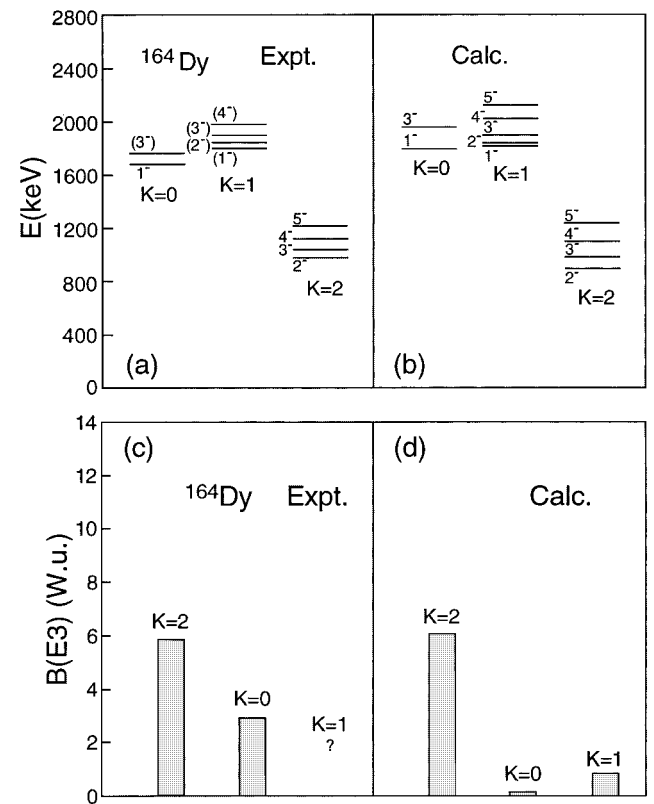
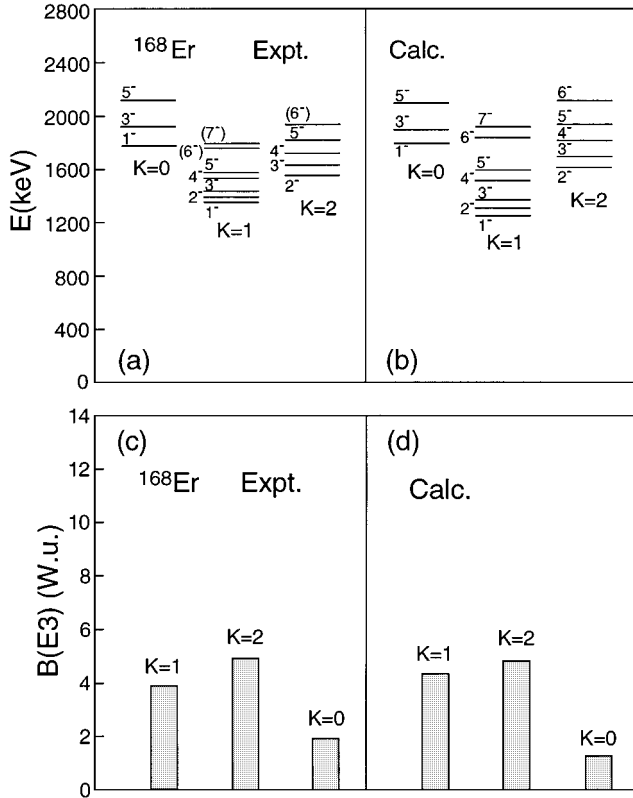


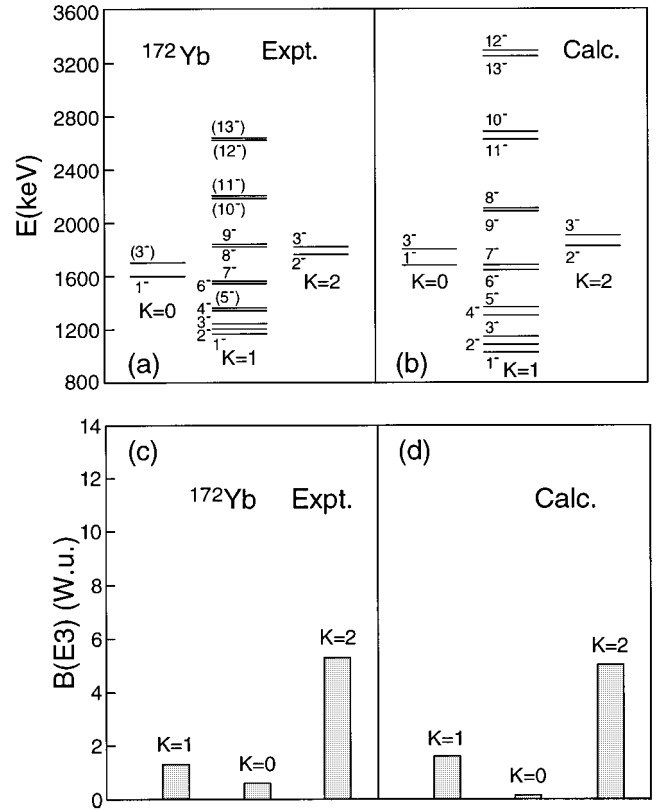
FIG. 8. Similar to Fig. 3 for ^{164}Dy [14,31].

FIG. 9. Similar to Fig. 3 for ^{168}Er [15,32].

difficulty, and noted that a large two quasineutron admixture (from the $5/2^+[642\uparrow]$ and $5/2^-[523\downarrow]$ Nilsson levels) has been predicted for the $K^\pi=0^-$ band in this nucleus by Soloviev [35]. More recently, this large two quasineutron admixture has been measured using the $^{161}\text{Dy}(d,p)^{162}\text{Dy}$ and $^{161}\text{Dy}(\alpha,^3\text{He})^{162}\text{Dy}$ reactions [36,37]. This would explain the low energy of the $K^\pi=0^-$ band since the neutron Fermi level is located between these two adjacent Nilsson orbits. This microscopic situation cannot be accommodated in the present model. In ^{160}Dy the $K^\pi=0^-$ band is calculated to be 500 keV higher than it is observed. In ^{164}Dy the calculated energies for the $K^\pi=0^-$ band are only 150 keV above the experimental results, suggesting smaller two-quasineutron admixtures. A measurement of the $^{163}\text{Dy}(d,p)^{164}\text{Dy}$ reaction would provide information about the two-quasineutron contribution to the $K^\pi=0^-$ states in ^{164}Dy . It should be noted that the parameters for $^{160,162,164}\text{Dy}$ in the present calculations were selected primarily to fit the $K^\pi=1^-$ and 2^- bands so that the anomalous locations of the $K^\pi=0^-$ bands would not distort the calculations.

The $B(E3)$ relative and absolute strengths are well reproduced except for $B(E3; 0_{\text{gs}}^+ \rightarrow 3_{K=0}^-)$ in $^{156,158}\text{Gd}$ and $^{162,164}\text{Dy}$ where the calculated values are significantly smaller than the data. Despite these disagreements, the general trends of the total $B(E3)$ strength and the individual octupole strengths for different K values from ^{154}Sm to ^{172}Yb are well reproduced.

The method used here for setting ϵ_f is one way of introducing microscopic information into the IBA, which does not intrinsically include details of single-particle configurations. From the behavior of the other parameters, it is clear that the importance of shell effects goes beyond the behavior of the octupole centroids. However, the present prescription

FIG. 10. Similar to Fig. 3 for ^{172}Yb [16,33].

for setting ϵ_f significantly constrains the model, and in fact determines a *unique* parameter set (A_2 and A_3) for fitting the energies of octupole band states. The results given here demonstrate that the fits that can be obtained with the systematic ϵ_f prescription are comparable to those given in [1].

IV. $E1$ TRANSITIONS

Electric dipole transitions from octupole vibration states depend not only on the structure of the octupole states but also on small admixtures of the giant dipole resonance [38]. We calculated $E1$ transitions using an operator which includes the effect of small giant dipole resonance admixtures [38] and is constrained to reproduce branching ratios given by the Alaga rules for pure states of good K quantum number [39]:

$$T_{sdf}^{(E1)} = e_1 [(d^\dagger f + d f^\dagger)^{(1)} + \chi_1 O_1 + \chi'_1 O'_1], \quad (14)$$

where O_1 and O'_1 are two-body terms. It was found [39] that the Alaga rule constraint required that $\chi_1 = 2\chi'_1$.

We first analyzed branching ratios of $E1$ transitions, for which the $E1$ effective charge e_1 cancels out, in order to focus on the parameters χ_1 and χ'_1 . To satisfy the Alaga rule constraint, we made only small deviations from the ratio $\chi_1/\chi'_1=2$ to fit the experimental $E1$ ratios.

The parameters χ_1 and χ'_1 used for each nucleus are listed in Table II, and the results of the calculations are compared to the experimental data in Tables III–X. In general, the calculations reproduce the experimental $B(E1)$ ratios well, and correctly follow the behavior as a function of spin within individual bands. Two cases for which data were available

TABLE III. $B(E1; J_i^- \rightarrow J_{f1}^+)/B(E1; J_i^- \rightarrow J_{f2}^+)$ for octupole bands in ^{154}Sm . Data are taken from [26].

| K^π | J_i^π | J_{f1}^π | J_{f2}^π | Expt. | Calc. |
|---------|-----------|--------------|-------------------|----------|-------|
| 0^- | 1^- | 2_1^+ | 0_{gs}^+ | 2.03(7) | 1.90 |
| | 3^- | 4_1^+ | 2_1^+ | 1.17(3) | 1.15 |
| | 5^- | 6_1^+ | 4_1^+ | 0.86(3) | 0.90 |
| 1^- | 1^- | 2_1^+ | 0_{gs}^+ | 237 | 3.7 |
| | 3^- | 4_1^+ | 2_1^+ | 5.58(55) | 2.8 |
| | 5^- | 6_1^+ | 4_1^+ | 4.60(60) | 50 |

over a larger range of spins, the $K^\pi=1^-$ bands in ^{156}Gd and ^{172}Yb , are shown in Fig. 11. In addition, the variation in $B(E1)$ ratios from nucleus to nucleus are well reproduced. Figure 12 illustrates branching ratios for $J^\pi=3^-$ states of $K^\pi=0^-, 1^-, 2^-$ bands for the nuclei studied here. The branching ratios for a given K value have the same order of magnitude as each other but there are small variations depending on the details of structure of each nucleus. The IBA reproduces these variations quite well with practically no free parameters in the $E1$ operator.

We also calculated absolute $B(E1)$ values of transitions for which data are available. In every case, the effective charge for the nucleus was set by fitting the calculated $B(E1)$ values to the data for the $1_{K=0}^- \rightarrow 0_{\text{gs}}^+$ and $1_{K=0}^- \rightarrow 2_1^+$ transitions. For ^{154}Sm , $^{156,158}\text{Gd}$, $^{160,162}\text{Dy}$, and ^{168}Er , these calculations allowed us to compare $E1$ transitions from different states. The calculated and experimental [29,30,32,33,40–42] $B(E1)$ values are listed in Table XI.

In two of these nuclei, ^{154}Sm and ^{156}Gd , the calculations reproduce the absolute $B(E1)$ data very well. In ^{158}Gd , the calculated $E1$ transitions from the $K^\pi=1^- J^\pi=3^-$ state are an order of magnitude larger than the data because the calculations give too much mixing between the $K^\pi=0^-$ and 1^- bands. In ^{160}Dy , the calculated $B(E1)$ values for transi-

TABLE IV. $B(E1; J_1^- \rightarrow J_{f1}^+)/B(E1; J_1^- \rightarrow J_{f2}^+)$ for octupole bands in ^{156}Gd . Data are taken from [27].

| K^π | J_1^π | J_{f1}^π | J_{f2}^π | Expt. | Calc. |
|---------|-----------|--------------|-------------------|----------------|----------|
| 1^- | 1^- | 2_1^+ | 0_{gs}^+ | 1.29(2) | 1.23 |
| | 3^- | 4_1^+ | 2_1^+ | 0.76(4) | 0.88 |
| | 5^- | 6_1^+ | 4_1^+ | 0.74(7) | 0.73 |
| | 7^- | 8_1^+ | 6_1^+ | ≈ 1.27 | 0.62 |
| | 9^- | 10_1^+ | 8_1^+ | 0.43(18) | 0.53 |
| | 11^- | 12_1^+ | 10_1^+ | < 6.88 | 0.44 |
| 0^- | 1^- | 2_1^+ | 0_{gs}^+ | 2.25(3) | 2.22 |
| | 3^- | 4_1^+ | 2_1^+ | 1.66(15) | 1.70 |
| 2^- | 2^- | 3_1^+ | 2_2^+ | 0.49(3) | 0.46 |
| | 3^- | 4_2^+ | 3_1^+ | 1.21(8) | 1.01 |
| | 3^- | 3_1^+ | 2_2^+ | 1.33(7) | 1.80 |
| | 3^- | 4_2^+ | 4_1^+ | 49(7) | ∞ |
| | 3^- | 2_2^+ | 2_1^+ | 22(2) | 6.8 |
| | 3^- | 4_1^+ | 2_1^+ | 0.72(10) | 0 |
| | 4^- | 5_1^+ | 4_2^+ | 1.94(17) | 1.73 |
| | 4^- | 4_2^+ | 3_1^+ | 0.53(4) | 0.78 |
| | 5^- | 5_1^+ | 4_2^+ | < 0.51 | 0.49 |

TABLE V. $B(E1; J_i^- \rightarrow J_{f1}^+)/B(E1; J_i^- \rightarrow J_{f2}^+)$ for octupole bands in ^{158}Gd . Data are taken from [28].

| K^π | J_i^π | J_{f1}^π | J_{f2}^π | Expt. | Calc. |
|---------|-----------|--------------|-------------------|----------|---------|
| 1^- | 1^- | 2_1^+ | 0_{gs}^+ | 0.98(7) | 1.11 |
| | 3^- | 4_1^+ | 2_1^+ | 0.88(2) | 0.88 |
| | 5^- | 6_1^+ | 4_1^+ | 0.80(7) | 0.76 |
| 0^- | 1^- | 2_1^+ | 0_{gs}^+ | 1.79(15) | 2.12 |
| | 3^- | 4_1^+ | 2_1^+ | 1.32(11) | 1.54 |
| | 5^- | 6_1^+ | 4_1^+ | 0.65(11) | 1.64 |
| | 2^- | 2^- | 3_1^+ | 2_2^+ | 0.59(5) |
| 2^- | 2^- | 2_2^+ | 2_1^+ | 490(59) | 103 |
| | 3^- | 4_2^+ | 3_1^+ | 1.33(11) | 1.04 |
| | 3^- | 3_1^+ | 2_2^+ | 1.58(13) | 1.66 |
| | 3^- | 2_2^+ | 2_1^+ | 12.6(20) | 11.6 |
| | 4^- | 4_2^+ | 3_1^+ | 0.29(6) | 0.82 |
| | 4^- | 4_2^+ | 4_1^+ | 0.71(16) | 13.1 |

tions from the $K^\pi=1^- J^\pi=2^-$ state are larger than the data, although they are still calculated to be small relative to the allowed $K^\pi=0^- \rightarrow K^\pi=0_{\text{gs}}^+$ transitions. In ^{162}Dy , the allowed $K^\pi=2^- \rightarrow K^\pi=2_\gamma^+$ transitions are calculated to be very strong, even significantly stronger than the $K^\pi=0^- \rightarrow K^\pi=0_{\text{gs}}^+$ transitions. However, the data show that the $K^\pi=2^- \rightarrow K^\pi=2_\gamma^+$ transitions are several orders of magnitude weaker than the $K^\pi=0^- \rightarrow K^\pi=0_{\text{gs}}^+$ transitions. In ^{168}Er , the calculated $B(E1)$ values for the transitions from the $K^\pi=1^- J^\pi=3^-$ state to the $K^\pi=0_{\text{gs}}^+$, $J^\pi=2^+, 3^+, 4^+$ states are significantly larger than the experimental values, but this problem does not occur in the

TABLE VI. $B(E1; J_i^- \rightarrow J_{f1}^+)/B(E1; J_i^- \rightarrow J_{f2}^+)$ for octupole bands in ^{160}Dy . Data are taken from [29].

| K^π | J_i^π | J_{f1}^π | J_{f2}^π | Expt. | Calc. |
|---------|-----------|--------------|-------------------|----------------|----------|
| 2^- | 2^- | 3_1^+ | 2_2^+ | 0.42(1) | 0.49 |
| | 2^- | 2_2^+ | 2_1^+ | 104(1) | 60 |
| | 3^- | 3_1^+ | 2_1^+ | 0.64(27) | 1.89 |
| | 3^- | 4_1^+ | 2_1^+ | 0.74(1) | 1.06 |
| | 4^- | 4_2^+ | 3_1^+ | 0.74(1) | 0.88 |
| | 4^- | 4_2^+ | 4_1^+ | 15(2) | 5.52 |
| | 5^- | 6_1^+ | 4_1^+ | < 3.99 | 2.54 |
| | 6^- | 5_1^+ | 6_1^+ | 9.38 | 4.30 |
| 1^- | 8^- | 7_1^+ | 8_1^+ | 17 | 3.38 |
| | 2^- | 3_1^+ | 2_2^+ | 1.32(1) | 23 |
| | 2^- | 2_2^+ | 2_1^+ | 6.09(4) | ∞ |
| | 3^- | 4_2^+ | 3_1^+ | 1.42(19) | ∞ |
| | 3^- | 3_1^+ | 2_2^+ | 1.19(9) | 0 |
| | 3^- | 4_2^+ | 4_1^+ | 0.44(5) | 0.38 |
| | 3^- | 2_2^+ | 2_1^+ | 0.23(1) | 0.014 |
| | 3^- | 4_1^+ | 2_1^+ | 0.91(1) | 1.51 |
| | 4^- | 5_1^+ | 4_2^+ | 5.48(41) | 2.02 |
| | 4^- | 4_2^+ | 3_1^+ | 0.37(2) | 1.00 |
| 0^- | 4^- | 4_2^+ | 4_1^+ | 5.13(33) | 8.80 |
| | 1^- | 2_1^+ | 0_{gs}^+ | 1.75(35) | 1.85 |
| | 3^- | 4_2^+ | 3_1^+ | ≈ 11.4 | 0.12 |
| | 3^- | 3_1^+ | 2_2^+ | ≈ 0.49 | 3.78 |

TABLE VII. $B(E1; J_i^- \rightarrow J_{f1}^+)/B(E1; J_i^- \rightarrow J_{f2}^+)$ for octupole bands in ^{162}Dy . Data are taken from [30,36].

| K^π | J_i^π | J_{f1}^π | J_{f2}^π | Expt. | Calc. | |
|---------|-----------|--------------|--------------|-------------------|-------------|------|
| 2^- | 2^- | 3_1^+ | 2_2^+ | 0.50(3) | 0.50 | |
| | | 3^- | 4_2^+ | 3_1^+ | 1.04(18) | 1.18 |
| | | 3^- | 3_1^+ | 2_2^+ | 1.55(35) | 1.89 |
| | | 3^- | 4_2^+ | 4_1^+ | 8.60(177) | 43 |
| | | 3^- | 2_2^+ | 2_1^+ | 5.92(150) | 11.9 |
| | | 3^- | 4_1^+ | 2_1^+ | 1.11(24) | 0.62 |
| | | 4^- | 5_1^+ | 4_2^+ | 1.72(40) | 2.08 |
| | | 4^- | 4_2^+ | 3_1^+ | 0.62(13) | 0.91 |
| | | 4^- | 5_1^+ | 4_1^+ | 1289(309) | 11.1 |
| | | 4^- | 4_2^+ | 4_1^+ | 626(167) | 5.34 |
| | | 4^- | 4_1^+ | 3_1^+ | 0.00063(13) | 0.17 |
| | | 5^- | 5_1^+ | 4_2^+ | 0.12(5) | 0.63 |
| | | 5^- | 6_1^+ | 4_1^+ | 0.90(10) | 0.64 |
| | | 5^- | 4_2^+ | 4_1^+ | 4.75(121) | 7.47 |
| | 0^- | 1^- | 2_1^+ | 0_{gs}^+ | 2.34(64) | 1.73 |
| 3^- | | 4_1^+ | 2_1^+ | 0.73(23) | 0.96 | |
| 5^- | | 6_1^+ | 4_1^+ | 0.86(24) | ∞ | |
| 5^- | | 4_2^+ | 4_1^+ | 1.68(21) | ∞ | |
| 1^- | 2^- | 3_1^+ | 2_1^+ | 5.31(67) | 6.0 | |
| | 2^- | 3_1^+ | 2_2^+ | 0.91(21) | 2.0 | |
| | 2^- | 2_2^+ | 2_1^+ | 8.20(175) | 3.0 | |
| | 3^- | 4_2^+ | 2_2^+ | 2.02(25) | 33 | |
| | 3^- | 4_2^+ | 4_1^+ | 17.7(29) | 0.52 | |
| | 3^- | 2_2^+ | 2_1^+ | 54.5(164) | 0.038 | |
| | 4^- | 5_1^+ | 4_1^+ | 8.13(114) | 0.75 | |
| | 5^- | 5_1^+ | 4_2^+ | 0.54(10) | 0.25 | |
| | 5^- | 6_1^+ | 4_1^+ | 2.83(100) | 1.32 | |
| | 5^- | 6_1^+ | 5_1^+ | 0.22(5) | 4.17 | |
| | 5^- | 4_2^+ | 4_1^+ | 24.2(804) | 0.13 | |

 TABLE VIII. $B(E1; J_i^- \rightarrow J_{f1}^+)/B(E1; J_i^- \rightarrow J_{f2}^+)$ for octupole bands in ^{164}Dy . Data are taken from [31].

| K^π | J_i^π | J_{f1}^π | J_{f2}^π | Expt. | Calc. | |
|---------|-----------|--------------|-------------------|----------|------------|------|
| 2^- | 2^- | 3_1^+ | 2_2^+ | 0.56(5) | 0.50 | |
| | | 2^- | 2_2^+ | 2_1^+ | 4932(1644) | 65 |
| | | 3^- | 4_2^+ | 3_1^+ | 1.26(31) | 1.18 |
| | | 3^- | 3_1^+ | 2_2^+ | 1.64(30) | 1.89 |
| | | 3^- | 4_2^+ | 4_1^+ | 487(257) | 43 |
| | | 3^- | 2_2^+ | 2_1^+ | 234(65) | 13.3 |
| | | 3^- | 4_1^+ | 2_1^+ | 0.99(57) | 0.68 |
| | | 4^- | 5_1^+ | 4_2^+ | 1.76(79) | 2.08 |
| | | 4^- | 4_2^+ | 3_1^+ | 0.69(15) | 0.92 |
| | | 5^- | 5_1^+ | 4_2^+ | 0.88(44) | 0.64 |
| | | 5^- | 4_2^+ | 4_1^+ | 68(14) | 8.0 |
| | | 5^- | 6_1^+ | 4_1^+ | <1.51 | 0.68 |
| 1^- | 1^- | 2_1^+ | 0_{gs}^+ | 1.38(30) | 1.5 | |
| | 3^- | 4_1^+ | 2_1^+ | 0.94(49) | 1.00 | |
| 0^- | 3^- | 4_1^+ | 2_1^+ | 1.76 | 0.0 | |

 TABLE IX. $B(E1; J_i^- \rightarrow J_{f1}^+)/B(E1; J_i^- \rightarrow J_{f2}^+)$ for octupole bands in ^{168}Er . Data are taken from [32].

| K^π | J_i^π | J_{f1}^π | J_{f2}^π | Expt. | Calc. | |
|---------|-----------|--------------|--------------|-------------------|-----------|----------|
| 1^- | 1^- | 2_2^+ | 2_1^+ | 0.15(3) | 0.52 | |
| | | 1^- | 2_1^+ | 0_{gs}^+ | 3.75(32) | 5.07 |
| | | 2^- | 3_1^+ | 2_2^+ | 0.15(3) | ∞ |
| | | 2^- | 2_2^+ | 2_1^+ | 3.51(57) | 0 |
| | | 3^- | 4_1^+ | 2_1^+ | 1.52(21) | 1.56 |
| | | 3^- | 3_1^+ | 2_2^+ | 0.056(11) | 0.010 |
| | | 4^- | 4_2^+ | 3_1^+ | 2.71(75) | 0.20 |
| | | 4^- | 4_2^+ | 4_1^+ | 3.57(89) | ∞ |
| | | 5^- | 6_1^+ | 4_1^+ | 1.19(18) | 1.09 |
| | | 6^- | 6_2^+ | 5_1^+ | 0.70(12) | 0.55 |
| | | 6^- | 6_2^+ | 6_1^+ | 1.68(36) | 4.00 |
| | | 7^- | 8_1^+ | 6_1^+ | 2.62(84) | 0.89 |
| | 2^- | 2^- | 3_1^+ | 2_2^+ | 0.52(3) | 0.48 |
| | | 2^- | 2_2^+ | 2_1^+ | 1577(100) | 95 |
| | | 3^- | 4_2^+ | 3_1^+ | 1.03(15) | 1.10 |
| 3^- | | 3_1^+ | 2_2^+ | 1.59(26) | 1.72 | |
| 3^- | | 2_2^+ | 2_1^+ | 1469(755) | ∞ | |
| 4^- | | 5_1^+ | 4_2^+ | 3.00(50) | 1.98 | |
| 4^- | | 4_2^+ | 3_1^+ | 0.57(10) | 0.78 | |
| 5^- | | 6_2^+ | 5_1^+ | 3.78(80) | 2.40 | |
| 5^- | | 5_1^+ | 4_2^+ | 0.35(6) | 0.52 | |
| 6^- | | 7_1^+ | 6_2^+ | 6.18(138) | 3.95 | |
| 6^- | | 6_2^+ | 5_1^+ | 0.25(7) | 0.34 | |
| 0^- | | 1^- | 2_1^+ | 0_{gs}^+ | 3.28(90) | 1.87 |
| | 3^- | 3_1^+ | 2_1^+ | 0.31(11) | 0.0036 | |
| | 3^- | 4_1^+ | 2_1^+ | 1.72(40) | 1.08 | |
| | 5^- | 6_2^+ | 6_1^+ | 1.05(19) | 0.039 | |
| | 5^- | 6_1^+ | 4_1^+ | 1.56(33) | 0.71 | |

transition from the $K^\pi = 1^-$, $J^\pi = 4^-$ state to the 4^+ state of the ground band. Overall, most experimental absolute $B(E1)$ values are well reproduced by the calculations, even though these quantities are very sensitive to small components in the wave functions.

Figure 13 compares the results of calculations and experiments for the $1^- \rightarrow 0_{\text{gs}}^+$ transitions and shows predictions for $1^- \rightarrow 0_{\text{gs}}^+$ $E1$ transitions which have not yet been measured.

 TABLE X. $B(E1; J_i^- \rightarrow J_{f1}^+)/B(E1; J_i^- \rightarrow J_{f2}^+)$ for octupole bands in ^{172}Yb . Data are taken from [33].

| K^π | J_i^π | J_{f1}^π | J_{f2}^π | Expt. | Calc. | |
|---------|-----------|--------------|-------------------|-----------|----------|------|
| 1^- | 1^- | 2_1^+ | 0_{gs}^+ | 6.54(24) | 9.18 | |
| | | 3^- | 4_1^+ | 2_1^+ | 2.00(18) | 2.03 |
| | | 5^- | 6_1^+ | 4_1^+ | 1.34(15) | 1.41 |
| | | 7^- | 8_1^+ | 6_1^+ | 1.76(25) | 1.15 |
| | | 9^- | 10_1^+ | 8_1^+ | 1.16(39) | 0.98 |
| 0^- | 1^- | 2_1^+ | 0_{gs}^+ | 1.79(15) | 1.96 | |
| | 3^- | 4_1^+ | 2_1^+ | 0.84(12) | 1.28 | |
| 2^- | 2^- | 3_1^+ | 2_2^+ | 0.76(14) | 0.49 | |
| | 2^- | 2_2^+ | 2_1^+ | 136(34) | 135 | |
| | 3^- | 3_1^+ | 2_1^+ | 26.2(136) | 20.4 | |

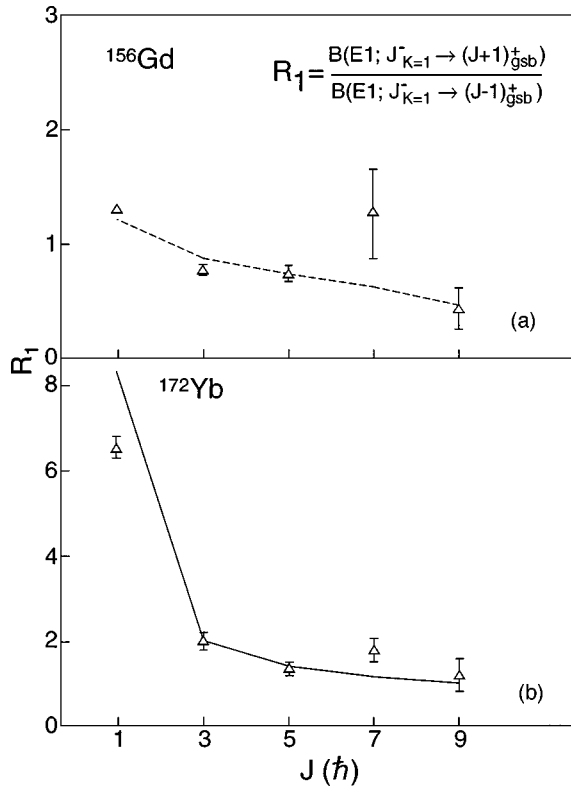


FIG. 11. Observed and calculated $E1$ branching ratios from $K^\pi=1^-$ band in (a) ^{156}Gd . Data are taken from [27]; (b) ^{172}Yb . Data are taken from [33].

The calculations reproduce rather well the almost constant $E1$ strength of the $1_{K=0}^- \rightarrow 0_{\text{gs}}^+$ transitions across the entire set of nuclei. In addition, the calculations predict very small values for $1_{K=1}^- \rightarrow 0_{\text{gs}}^+$ transitions ($10^{-3} - 10^{-5} e^2 \text{fm}^2$) for all these nuclei except for ^{156}Gd , which is in fact the only case where this quantity has been measured. The large value of $1_{K=1}^- \rightarrow 0_{\text{gs}}^+$ in ^{156}Gd is due to the strong mixing of the $K=0$ and $K=1$ bands in this nucleus (see Fig. 2 and [23]). Data on $1^- \rightarrow 0_{\text{gs}}^+$ transitions which have not yet been measured will provide rigorous tests of the present calculations.

V. $K^\pi=3^-$ BANDS

While the data on energies and $B(E3)$ values for $K^\pi=0^-, 1^-, 2^-$ bands are reasonably complete for the eight nuclei discussed here, the data on $K^\pi=3^-$ bands are limited and questionable. At this time, the best candidate for a $K^\pi=3^-$ octupole band is the band based on the 2262.7 keV state in ^{168}Er . With this state, there is evidence for both a $K^\pi=3^-$ band structure and a large $B(E3; 0_{\text{gs}}^+ \rightarrow 3^-)$ value. Davidson and Dixon [43] argued that the 2262.7 keV state must have $J^\pi=3^-$ because of the spins and parities of the states ($2^+, 3^+, 3^-, 4^+$, and 4^-) to which it deexcites. Govil *et al.* [15] measured $B(E3; 0_{\text{gs}}^+ \rightarrow 3^-) = 4.7$ Weisskopf units (W.u.), in the (α, α') reaction at 36 MeV. However, Jungclaus *et al.* [44] questioned the $J^\pi=3^-$ assignment for the 2262.7 keV bandhead. Davidson and Dixon [43] reported that the 2262.7 keV state decays to a 2^+ state (at 821 keV), but Jungclaus *et al.* [44] did not see the transition to this

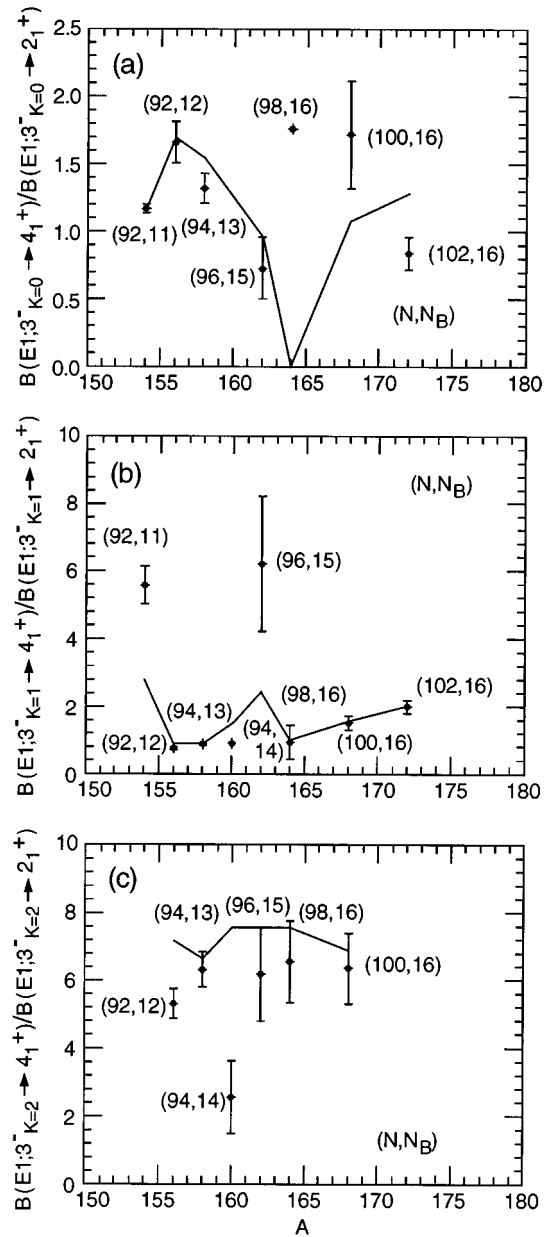


FIG. 12. Observed (points) and calculated (line) $E1$ branching ratios from $J^\pi=3^-$ states in the (a) $K^\pi=0^-$, (b) $K^\pi=1^-$, and (c) $K^\pi=2^-$ octupole bands in the eight nuclei studied here. The neutron and boson numbers (N, N_B) are indicated for each nucleus.

state in their high statistics coincidence experiment. Consequently, they argued that a $J^\pi=4^-$ assignment could not be excluded.

Davidson and Dixon [43] also identified five other $K^\pi=3^-$ bands in ^{168}Er , with band-heads at 1541, 1828, 1999, 2323, and 2337 keV. However, the $B(E3; 0_{\text{gs}}^+ \rightarrow 3^-)$ values measured for the lowest four of these states in the (α, α') reaction [15] are small, being only 0.25, 0.60, 0.42, and 1.53 W.u., respectively, suggestive of a noncollective origin. The corresponding matrix element for the 2337 keV state has not been measured. Data from the $^{167}\text{Er}(d, p)$ reaction also support the noncollective interpretation of the 1541 and 1828 keV states [45].

TABLE XI. $B(E1; J_i^- \rightarrow J_f^+)$ values.

| Nucleus | e_1 (e fm) | K^π | J_i^π | J_f^π | Expt. ($e^2 \text{fm}^2$) | Calc. ($e^2 \text{fm}^2$) | Ref. |
|-------------------|--------------|---------|-----------|-------------------|-----------------------------|-----------------------------|------|
| ^{154}Sm | 0.32 | 0^- | 1^- | 0_{gs}^+ | $1.15(8) \times 10^{-2}$ | 1.11×10^{-2} | [40] |
| | | 0^- | 1^- | 2_1^+ | $2.17(48) \times 10^{-2}$ | 2.10×10^{-2} | [40] |
| | | 0^- | 3^- | 2_1^+ | $1.44(18) \times 10^{-2}$ | 1.54×10^{-2} | [40] |
| ^{156}Gd | 0.28 | 0^- | 3^- | 4_1^+ | $1.73(26) \times 10^{-2}$ | 1.77×10^{-2} | [40] |
| | | 1^- | 1^- | 0_{gs}^+ | $3.33(133) \times 10^{-3}$ | 3.32×10^{-3} | [41] |
| | | 1^- | 1^- | 2_1^+ | $4.30(172) \times 10^{-3}$ | 4.08×10^{-3} | [41] |
| ^{158}Gd | 0.25 | 0^- | 1^- | 0_{gs}^+ | $5.33(197) \times 10^{-3}$ | 5.54×10^{-3} | [41] |
| | | 0^- | 1^- | 2_1^+ | $1.20(44) \times 10^{-2}$ | 1.23×10^{-2} | [41] |
| | | 1^- | 3^- | 4_1^+ | $5.3(17) \times 10^{-4}$ | 5.86×10^{-3} | [28] |
| ^{160}Dy | 0.43 | 1^- | 3^- | 2_1^+ | $6.2(19) \times 10^{-4}$ | 6.66×10^{-3} | [28] |
| | | 0^- | 1^- | 0_{gs}^+ | $6.63(156) \times 10^{-3}$ | 5.98×10^{-3} | [41] |
| | | 0^- | 1^- | 2_1^+ | $1.19(30) \times 10^{-2}$ | 1.27×10^{-2} | [41] |
| ^{162}Dy | 1.96 | 2^- | 3^- | 4_1^+ | $5.9(17) \times 10^{-4}$ | 3.33×10^{-4} | [29] |
| | | 2^- | 3^- | 2_1^+ | $8.0(23) \times 10^{-4}$ | 3.14×10^{-4} | [29] |
| | | 1^- | 2^- | 3_1^+ | $4.7(2) \times 10^{-7}$ | 4.25×10^{-4} | [29] |
| | | 1^- | 2^- | 2_2^+ | $3.6(2) \times 10^{-7}$ | 1.85×10^{-5} | [29] |
| | | 1^- | 2^- | 2_1^+ | $5.9(3) \times 10^{-8}$ | 0 | [29] |
| | | 0^- | 1^- | 2_1^+ | $1.3(3) \times 10^{-2}$ | 1.29×10^{-2} | [29] |
| | | 0^- | 1^- | 0_{gs}^+ | $7.2(8) \times 10^{-3}$ | 6.95×10^{-3} | [29] |
| ^{164}Dy | 5.36 | 2^- | 2^- | 3_1^+ | $4.8(10) \times 10^{-5}$ | 1.59×10^{-1} | [30] |
| | | 2^- | 2^- | 2_2^+ | $9.6(19) \times 10^{-5}$ | 3.18×10^{-1} | [30] |
| | | 2^- | 2^- | 2_1^+ | $9.8(19) \times 10^{-9}$ | 5.38×10^{-3} | [30] |
| ^{168}Er | 0.29 | 0^- | 1^- | 0_{gs}^+ | $4.9(8) \times 10^{-3}$ | 5.76×10^{-3} | [30] |
| | | 0^- | 1^- | 2_1^+ | $1.15(37) \times 10^{-2}$ | 1.00×10^{-2} | [30] |
| | | 0^- | 1^- | 0_{gs}^+ | $5.75(71) \times 10^{-3}$ | 5.70×10^{-3} | [42] |
| | | 1^- | 3^- | 3_1^+ | 1.2×10^{-7} | 1.68×10^{-5} | [32] |
| | | 1^- | 3^- | 4_1^+ | 3.3×10^{-6} | 2.51×10^{-3} | [32] |
| | | 1^- | 3^- | 2_1^+ | 2.2×10^{-6} | 1.61×10^{-3} | [32] |
| | | 1^- | 4^- | 4_2^+ | 2.0×10^{-5} | 0.84×10^{-5} | [32] |
| ^{172}Yb | 0.14 | 1^- | 4^- | 3_1^+ | 0.69×10^{-5} | 4.21×10^{-5} | [32] |
| | | 1^- | 4^- | 4_1^+ | 1.0×10^{-6} | 0 | [32] |
| | | 0^- | 1^- | 2_1^+ | $1.9(4) \times 10^{-2}$ | 1.46×10^{-2} | [32] |
| | | 0^- | 1^- | 0_{gs}^+ | $5.7(18) \times 10^{-3}$ | 7.84×10^{-3} | [32] |
| | | 0^- | 1^- | 2_1^+ | $6.4(18) \times 10^{-3}$ | 6.26×10^{-3} | [33] |
| | | 0^- | 1^- | 0_{gs}^+ | $3.6(10) \times 10^{-3}$ | 3.19×10^{-3} | [33] |
| | | 0^- | 1^- | 0_{gs}^+ | | | |

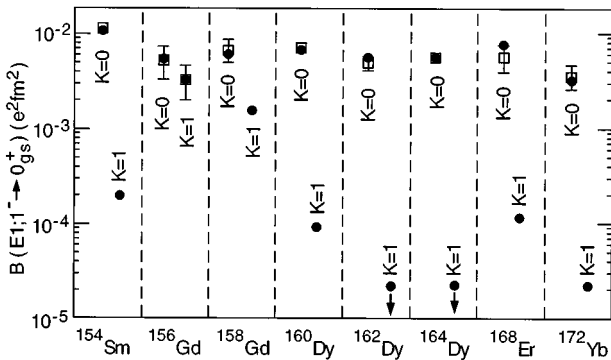


FIG. 13. Calculated (full circles) and experimental (open squares) $B(E1; 1^-_K \rightarrow 0^+_{\text{gs}})$ values for $K=0^-$ and 1^- . The calculated values without corresponding experimental points are predictions for transitions not yet measured.

$K^\pi=3^-$ bands have also been observed in ^{162}Dy , with bandheads at 1571 and 1767 keV [36,46]. However, these states appear to have small $B(E3; 0^+_{\text{gs}} \rightarrow 3^-)$ values because they were populated only weakly if at all in the (d, d') experiments of Grotdal *et al.* [14]. This suggests a non-collective interpretation. Govil *et al.* [16] measured a relatively large $B(E3; 0^+_{\text{gs}} \rightarrow 3^-)$ value (4.7 W.u.) for a state assigned to have $J^\pi=3^-$ at 2030 keV in ^{172}Yb and assigned $K^\pi=3^-$; however, there is no band structure established with this state, and therefore little evidence for the K^π assignment.

In the framework of the IBA-1, the behavior of $K^\pi=3^-$ octupole states can be predicted on the basis of the fits to the $K^\pi=0^-, 1^-$, and 2^- bands. This seems to be a reasonable thing to do given the experimental situation, and we proceed to do this here.

In the SU(3) limit of the sd Hamiltonian, the sd - f quadrupole-quadrupole interaction breaks the degeneracy of the negative parity states and develops different bands char-

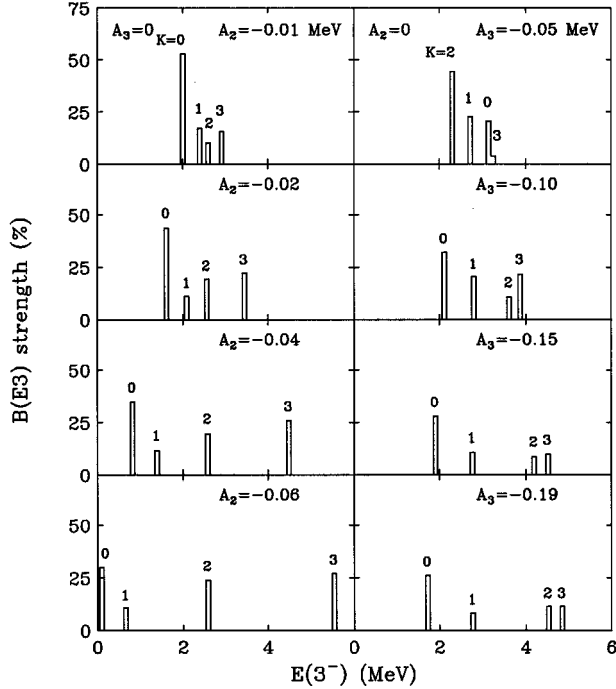


FIG. 14. The calculated energies and $E3$ strengths of the $J=3^-$ states of the $K^\pi=0^-, 1^-, 2^-$, and 3^- bands. The core corresponds to ^{168}Er as discussed in the text. Left: different values of A_2 . Right: different values of A_3 .

acterized by the quantum number K [47]. The splitting of the different bands is proportional to K^2 and to the strength of the sd - f quadrupole-quadrupole interaction A_2 . In particular, for large negative values of A_2 , the energy of the $I=3^-, K=3^-$ state based on the lowest $SU(3)$ irreducible representation of the positive parity core is pushed up in energy relative to the $I=3^-$ members of the $K=0^-, 1^-$, and 2^- bands built on the ground state according to the relation [1]:

$$E(K) = E_0 + (2N-2)(4-K^2)A_2/\sqrt{6}. \quad (15)$$

In the asymptotic limit, $N \rightarrow \infty$, $A_2 \rightarrow \infty$, if the $E3$ operator is $s^\dagger \tilde{f} + f^\dagger s$, the four bands, $K=0^-, 1^-, 2^-$, and 3^- are excited in the ratio 1:2:2:2 [47]. For a Hamiltonian corresponding to deformed nuclei but not in the $SU(3)$ limit this pattern is altered, but the $K=3^-$ state is still highest in energy. In Fig. 14 (left), the locations and octupole strengths of the $I=3^-$ states of the four bands are shown for different values of A_2 . The core corresponds to ^{168}Er : $N_B=16$, $a_1=6.5$ keV, $a_2=-17.5$ keV, and $\chi=-0.49$. An exchange term in the sd - f interaction produces a different octupole strength distribution, but for negative values of the strength of this interaction, A_3 , the $K=3^-$ state is again the highest in energy (Fig. 14, right). The presence of both interactions in the sd - f Hamiltonian, which is necessary to reproduce the ordering of the $K=0^-, 1^-$, and 2^- bands in deformed nuclei, and of a second term in the $E3$ operator $\chi_3(d^\dagger \tilde{f} + f^\dagger \tilde{d})^{(3)}$, which is required to reproduce the corresponding octupole strength distribution, does not modify this picture with the $K=3^-$ state at a very high excitation energy (Fig. 15).

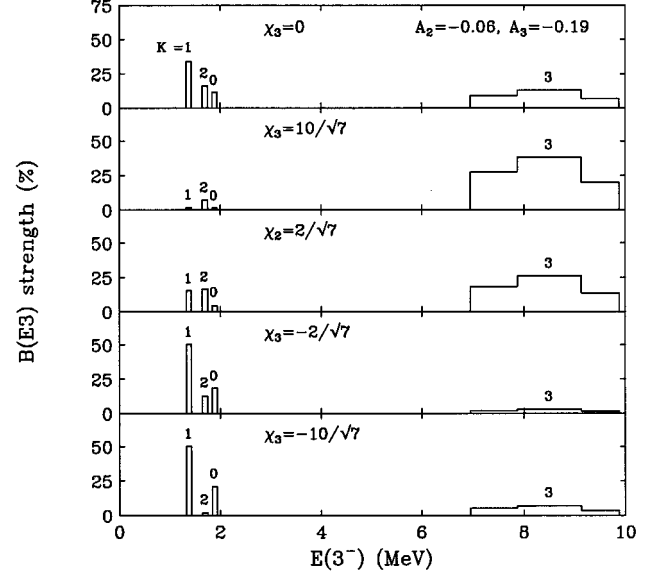


FIG. 15. The calculated $E3$ strength distributions of the $K^\pi=0^-, 1^-, 2^-$, and 3^- bands are shown for different values of χ_3 . The core corresponds to ^{168}Er .

In Fig. 16, the calculated octupole strength distributions for the eight nuclei discussed here are shown. For all these nuclei but ^{154}Sm , large $K=3$ strength occurs above 6 MeV (for ^{154}Sm the $K=3$ strength occurs at 4.3 MeV). This is approximately the same excitation energy ($31 A^{-1/3}$ MeV) at which the low energy octupole resonance (LEOR) is located. The LEOR is considered to be a $1\hbar\omega$ excitation [3]. Thus, the high energy $I=3^-, K=3^-$ octupole vibrational state based on the ground state is either experimentally masked by the LEOR or is the state which has been experimentally identified as the LEOR. In any case, the observed strength of this state provides a constraint on allowable Hamiltonian or octupole transition operators.

VI. SUMMARY

We have introduced a method for setting the parameter ϵ_f in the IBA-1 with f boson by using the systematic behavior of the centroids of observed $E3$ strength and applied it to octupole bands in eight deformed rare earth nuclei. The evolution of the ordering of the bands with different K quantum numbers and the $B(E3)$ and $B(E1)$ values associated with the different bands across the deformed region is well reproduced. The calculations are in good agreement with the data for nearly all the $K^\pi=0^-, 1^-$, and 2^- octupole bands in the nuclei studied here. The least satisfactory fits were obtained for the $K^\pi=0^-$ bands in $^{160,162}\text{Dy}$, although this can be explained as a consequence of the large noncollective contributions to these states. It is predicted that in $^{160,162,164}\text{Dy}$, ^{168}Er , and ^{172}Yb the $E3$ strength of the $K^\pi=3^-, J^\pi=3^-$ octupole vibrational state based on the ground state is concentrated above 6 MeV, the range in which the LEOR is located.

Octupole vibration states in deformed nuclei have been of interest for at least 25 years (for example, see [22]); nevertheless, there are still large deficiencies in the information available on distributions of $E3$ strength in these nuclei, par-

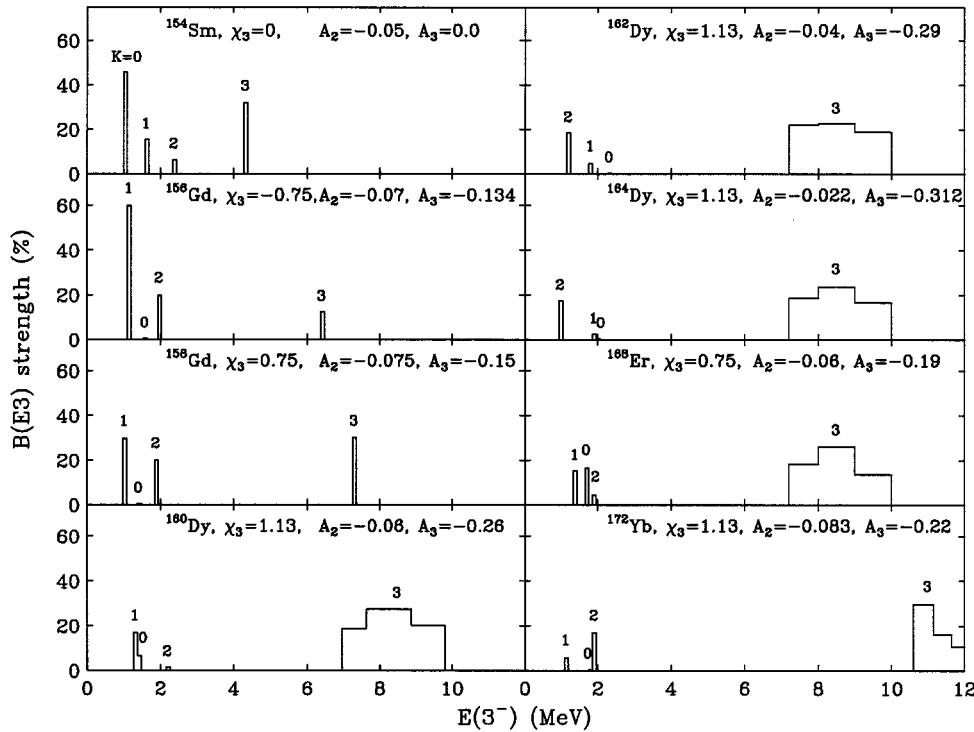


FIG. 16. Calculated $E3$ strength distributions for the $K^\pi=0^-, 1^-, 2^-,$ and 3^- octupole bands for all eight nuclei studied here.

ticularly with respect to $K^\pi=3^-$ octupole states. High resolution focal plane detectors now in use with magnetic spectrographs provide the opportunity for detailed systematic studies of octupole states, even in deformed nuclei where the density of states is high and the fragmentation of the octupole strength is significant. Such information would be of vital importance in determining whether the present version of the IBA can adequately describe octupole excitations in these nuclei.

ACKNOWLEDGMENTS

We are indebted to F. Iachello, R. F. Casten, and O. Scholten for valuable discussions. The present work was supported by the National Science Foundation, the Department of Energy under Contract Nos. DE-FG02-91ER40609, DE-AC02-76CH00016, and DE-FG02-88ER40417, and the State of Florida.

-
- [1] A.F. Barfield, J.L. Wood, and B.R. Barrett, *Phys. Rev. C* **34**, 2001 (1986); A.F. Barfield, B.R. Barrett, J.L. Wood, and O. Scholten, *Ann. Phys. (N.Y.)* **182**, 344 (1988).
- [2] P.D. Cottle, K.A. Stuckey, and K.W. Kemper, *Phys. Rev. C* **38**, 2843 (1988).
- [3] M.W. Kirson, *Phys. Lett.* **108B**, 237 (1982).
- [4] A. Arima and F. Iachello, *Phys. Lett.* **57B**, 39 (1975).
- [5] A. Arima and F. Iachello, *Ann. Phys. (N.Y.)* **111**, 201 (1978).
- [6] D.D. Warner and R.F. Casten, *Phys. Rev. Lett.* **48**, 1385 (1982).
- [7] F.T. Baker and R. Tickle, *Phys. Rev. C* **5**, 182 (1972).
- [8] M. Pignanelli, N. Blasi, J.A. Bordewijk, R. De Leo, M.N. Harakeh, M.A. Hofstee, S. Micheletti, R. Perrino, V.Yu. Ponomarev, V.G. Soloviev, A.V. Sushkov, and S.Y. van der Werf, *Nucl. Phys.* **A559**, 1 (1993).
- [9] E. Müller-Zanotti, R. Hertzenberger, H. Kader, D. Hofer, G. Graw, Gh. Cata-Danil, G. Lazzari, and P.F. Bortignon, *Phys. Rev. C* **47**, 2524 (1993).
- [10] M. Pignanelli, N. Blasi, S. Micheletti, R. De Leo, M.A. Hofstee, J.M. Schippers, S.Y. van der Werf, and M.N. Harakeh, *Nucl. Phys.* **A519**, 567 (1990).
- [11] E. Veje, B. Elbek, B. Herskind, and M.C. Olesen, *Nucl. Phys.* **A109**, 489 (1968).
- [12] G. de Angelis, P. Kleinheinz, B. Rubio, J.L. Tain, K. Zuber, B. Brinkmoller, P. von Rossen, J. Romer, D. Paul, J. Meissburger, G.P.A. Berg, A. Magiera, G. Hlawatsch, L.G. Mann, T.N. Massey, D. Decman, G.L. Struble, and J. Blomqvist, *Z. Phys.* **A 336**, 375 (1990).
- [13] R. Bloch, B. Elbek, and P.O. Tjom, *Nucl. Phys.* **A91**, 576 (1967).
- [14] T. Grottdal, K. Nybo, T. Thorsteinsen, and B. Elbek, *Nucl. Phys.* **A110**, 385 (1968).
- [15] I.M. Govil, H.W. Fulbright, D. Cline, E. Wesolowski, B. Kottlinski, A. Backlin, and K. Gridnev, *Phys. Rev. C* **33**, 793 (1986).
- [16] I.M. Govil, H.W. Fulbright, and D. Cline, *Phys. Rev. C* **36**, 1442 (1987).
- [17] R. Perrino, R. De Leo, A.D. Bacher, G.T. Emery, C.W. Glover, H. Nann, C. Olmer, R.V.F. Janssens, and S.Y. van der Werf, *Phys. Rev. C* **45**, 1017 (1992).
- [18] A. Hogenbirk, H.P. Blok, and M.N. Harakeh, *Nucl. Phys.* **A524**, 251 (1991).

- [19] J.E. Finck, G.M. Crawley, J.A. Nolen, Jr., and R.T. Kouzes, Nucl. Phys. **A407**, 163 (1983).
- [20] Y. Fujita, M. Fujiwara, S. Morinobu, I. Katayama, T. Yamazaki, T. Itahashi, H. Ikegami, and S.I. Hayakawa, Phys. Rev. C **32**, 425 (1985).
- [21] R.F. Casten, D.D. Warner, D.S. Brenner, and R.L. Gill, Phys. Rev. Lett. **47**, 1433 (1981).
- [22] K. Neergard and P. Vogel, Nucl. Phys. **A145**, 33 (1970).
- [23] R.F. Casten, W.T. Chou, and N.V. Zamfir, Nucl. Phys. **A555**, 563 (1993).
- [24] O. Scholten, The Program-Package PHINT, Kernfysisch Versneller Instituut Internal Report No. 63, 1979.
- [25] M. Sugawara, H. Kusakari, T. Morikawa, H. Inoue, Y. Yoshizawa, A. Virtanen, M. Piiparinen, and T. Horiguchi, Nucl. Phys. **A557**, 653c (1993).
- [26] R.G. Helmer, Nucl. Data Sheets **69**, 507 (1993).
- [27] R.G. Helmer, Nucl. Data Sheets **65**, 65 (1992).
- [28] M.A. Lee, Nucl. Data Sheets **56**, 199 (1989).
- [29] C.W. Reich, Nucl. Data Sheets **68**, 405 (1993).
- [30] R.G. Helmer, Nucl. Data Sheets **64**, 79 (1991).
- [31] E.N. Shurshikov and N.V. Timofeeva, Nucl. Data Sheets **65**, 365 (1992).
- [32] V.S. Shirley, Nucl. Data Sheets **71**, 261 (1994).
- [33] B. Singh, Nucl. Data Sheets **75**, 199 (1995).
- [34] P. Vogel, Phys. Lett. **60B**, 431 (1976).
- [35] V.G. Soloviev, Theory of Complex Nuclei (Pergamon, New York, 1976).
- [36] J. Berzins, P. Prokofjevs, R. Georgi, R. Hucce, T. von Egidy, G. Hlawatsch, J. Klora, H. Lindner, U. Mayerhofer, H.H. Schmidt, A. Walter, V.G. Soloviev, N.Yu. Shirikova, and A.V. Sushkov, Nucl. Phys. **A584**, 413 (1995).
- [37] E. Andersen, H. Helstrup, G. Lovhoiden, T.F. Thorsteinsen, M. Guttormsen, S. Messelt, T.S. Tvetter, M.A. Hofstee, J.M. Schippers, and S.Y. van der Werf, Nucl. Phys. **A550**, 235 (1992).
- [38] N.V. Zamfir, O. Scholten, and P. von Brentano, Z. Phys. A **337**, 293 (1990).
- [39] P. von Brentano, N.V. Zamfir, and A. Zilges, Phys. Lett. B **278**, 221 (1992).
- [40] A. Jungclaus, T. Belgya, D.P. DiPrete, M. Villani, E.L. Johnson, E.M. Baum, C.A. McGrath, S.W. Yates, and N.V. Zamfir, Phys. Rev. C **48**, 1005 (1993).
- [41] H.H. Pitz, U.E.P. Berg, R.D. Heil, U. Kneissl, R. Stock, C. Wesselborg, and P. von Brentano, Nucl. Phys. **A492**, 411 (1989).
- [42] J.A. Margraf, T. Eckert, M. Rittner, I. Bauske, O. Beck, U. Kneissl, H. Maser, H.H. Pitz, A. Schiller, P. von Brentano, R. Fisher, R.-D. Herzberg, N. Pietralla, A. Zilges, and H. Friedrichs, Phys. Rev. C **52**, 2429 (1995).
- [43] W.F. Davidson and W.R. Dixon, J. Phys. G **17**, 1683 (1991).
- [44] A. Jungclaus, R.F. Casten, R.L. Gill, and H.G. Borner, Phys. Rev. C **49**, 88 (1994).
- [45] D.G. Burke, B.L.W. Maddock, and W.F. Davidson, Nucl. Phys. **A442**, 424 (1985).
- [46] D.D. Warner, R.F. Casten, W.R. Kane, and W. Gelletly, Phys. Rev. C **27**, 2292 (1983).
- [47] F. Iachello and A. Arima, *The Interacting Boson Model* (Cambridge University Press, Cambridge, 1987).